The Effect of Temperature on Faceplate/Core Delamination in Composite/Titanium Sandwich Plates

Final Report on

National Aeronautics and Space Administration Contract

NCC-1-303

to

Dr. Tom Gates

NASA Langley Research Center

MS188E

Hampton, VA 23681

Engineering Mechanics Research Laboratory Report

EMRL 00/7

Kenneth M. Liechti and Balázs Marton

Research Center

Mechanics of Solids, Structures & Materials

Department of Aerospace Engineering and Engineering Mechanics

The University of Texas at Austin

Austin, TX 78712

September 2000

Abstract

A study was made of the delamination behavior of sandwich beams made of titanium core bonded to face-plates that consisted of carbon fiber reinforced polymer composite. Nominally mode I behavior was considered at 23 °C and 180 °C, by making use of a specially reinforced double cantilever (DCB) specimens. The toughness of the bond between the faceplate and the core was determined on the basis of a beam on elastic foundation analysis. The specimen compliance, and toughness were all independent of temperature in these relatively short-term experiments. The fracture mechanism showed temperature dependence, due to the hygrothermal sensivity of the adhesive.

Table of Contents

List of Figures

CHAPTER ONE

Introduction

Sandwich structures are desirable materials in aerospace structures, due to their low weight, high stiffness, durability and high strength. It has recently become possible to fabricate cores from titanium, instead of the traditional nomex aluminum. The greatest advantage of introducing titanium core is that sandwich structures can be used at higher temperatures. This means that the current bounds on air speed and altitude can be extended. Accurate knowledge of mechanical behavior of sandwich panels, such as critical buckling loads, mode shapes and debonding behavior is essential for reliable and lightweight structural design. One damage mode in sandwich panels is compressive delamination, where a delamination between the core and faceplate buckles and causes further growth of the delamination. One damage mode that can occur in sandwich panels is compressive delamination, where a delamination between the core and faceplate buckles and causes further growth of the delamination. Starting with the work of Chai et. al. (1981), this problem has been examined extensively in the composites delamination literature. Kassapoglou et. al. (1988) made the extension to composite sandwich structures, but not much work has been done since then, particularly at high temperatures.

A central component of any analysis will be the fracture resistance of the core/ faceplate bond. This essentially was the focus of this study and the review of related work which now follows.

It seems that Triantafillou and Gibson (1989) conducted the earliest examination of the fracture resistance faceplate/core interfaces. They examined mode I debonding in aluminum/foam sandwiches using simplified stress analyses and fracture mechanics energy principles. They examined transferability issues and found that core/interface cracks had to be quite long for debonding to occur. Carlsson, Senlein and Merry (1991) used a three-point bending configuration called a cracked sandwich beam (CSB) to determine faceplate/core toughness of glass/polyester faceplates on balsa core in mode II. Beam theory with shear deformation was used to determine the specimen compliance. Zenkert (1991) used CSB and end-notched flexure (ENF) specimens to respectively determine the toughness of the interface and the core itself. Fracture in four different beams in four-point bending was predicted on the basis of toughness values that had been determined. The predictions were quite reasonable once crack closure effects were accounted for. It was found that cracks significantly reduced the load carrying capability of the beams. Carlsson and Prassad (1993) presented an analysis of the effect of global peel loading, shear loading and residual stress on mixed-mode stress intensity factors at the faceplate/core interface. The effect of

modulus ratio and the possibility of crack kinking were examined. Core thickness had little effect on K_I but had a major influence on K_{II}. The effect of faceplate surface preparation (shot blast, sanding, pinning, etc.) on the bending load-deflection response of aluminum/reinforced resin sandwiches was considered by Bakos and Papanicolau (1993). It was found that emery paper and sandblast treatments provided the highest strength. Prasad and Carlsson (1994a) conducted a crack analysis of core/sandwich delamination in DCB and block shear configurations using interface fracture concepts. As expected, they found that K_I dominates in DCB specimens. However, in block shear and particularly with soft cores, there was no mode I effect. At the facing/bond and bond/core interfaces, the overall stress intensity increased with increasing core modulus. Core thickness did not have much effect. The possibility of kinking increased with compliant cores in mode I and can occur at any time with mode II. In experiments that followed the analysis just described, several core/faceplate combinations were considered (Prasad and Carlsson, 1994b). The toughness and kink angle for each combination was determined under nominally mode I and II conditions. Falk (1994) considered the issue of transferability. Predictions of delamination from a circular faceplate/core crack in a square sandwich panel, made on the basis of toughness values that were determined from an ENF specimen with a central core crack were quite reasonable. The panel failed via branching into the core. Papanicolau and Bakos (1995) followed up their earlier study of the effect of

surface treatment on the bending behavior of aluminum faceplate/composite core sandwiches with some Mode I fracture experiments. Several methods of extracting energy release rates were considered. A corrected beam theory was most consistent and rough surfaces provided the highest toughness. TerMaath, Ingraffea and Wawrzynek (1999) conducted a finite element analysis of faceplate/core debonding where the hexagonal structure of the core was explicitly modeled. A modified crack closure technique was used to determine energy release rates. Self-similar and self-repeating crack growth was considered and mesh convergence was checked. Parametric studies revealed that faceplate thickness and stiffness had the largest effect on energy release rate values. Li and Carlsson (1999) used a tilt specimen to probe the interface between the PVC foam core and glass/vinyl ester faceplates. The above a critical value, the tilt forces the crack to grow along the interface. The toughness of this interface was about 0.5 kJ/m^2. This paper was followed by an elastic foundation analysis of the tilt specimen (Li and Carlsson, 2000). Measured and predicted (beam on elastic foundation) compliance values were in good agreement. The toughness of the xxxxxx/yyyyy interface was 1.3 kJ/m^2 and several parametric studies were conducted.

The main objective of this work was to determine how faceplate debonding occurs under mode I loading in sandwich structures at room and high

temperatures. The approach that was taken was to determine the elastic properties of carbon fiber reinforced faceplates and the transverse tensile behavior of the sandwich and then conduct a series of fracture experiments over a range of temperatures. The experiments were accompanied by analyses that incorporated the elastic foundation behavior of the core and fracture calculations.

CHAPTER TWO

Experimental Procedures

Several different experiments were conducted in this study. Sandwich panels of composite faceplates bonded to titanium core were considered. The first series of experiments was used to determine the longitudinal Young's modulus and ultimate tensile strength of the faceplate material. The objective of the second series of experiments was to determine the transverse mechanical properties of a section of sandwich material. This experiment was referred to as the sandwich tension test. The third set of experiments dealt with the fracture resistance of the core/faceplate bond. The faceplate was peeled from the core using a specially designed fixture. These experiments were conducted at 23 and 180 °C.

2.1. Faceplate Behavior

The subject of this work was a IM7/PETI-5 sandwich panel with carbon fiber reinforced faceplates, titanium honeycomb core bonded with FMx5 film adhesive. Although the panels that were supplied contained some defects (crushed core, delaminations, etc.) there was plenty of material to work with. The layup of the faceplates was $[45/0/-45/90]_{2S}$ and the thickness of the sandwich plate was 25.4mm (1.0 in). They were carefully removed from the

core and cut into 266.7mm (10.5 in) long by 12.7 (0.5 in) wide by 1.27 mm (0.05 in) strips.

Two strain gages were attached to the middle of the strip. One measured the axial strain while the other was used for the lateral strain. Two-inch long tapered tabs were bonded to each side and end of the strips, to smoothly introduce the load from the hydraulic grips to the gage section. Experiments were conducted in a servo hydraulic loading device, in displacement control at a rate of 0.0254 mm/s (0.001 in/s). The load was measured with a 20,000 lb load-cell, the displacement was measured by a built-in Linear Voltage Differential Transformer (LVDT) at the bottom of the actuator piston. The data acquisition and experiment control was accomplished via computerized data acquisition system with 16-bit analog to digital conversion.

Four experiments were conducted; the first three were used to measure only elastic properties, while the fourth was a failure test, to measure the strength of the laminate. The axial stress-strain behavior is shown in Figure 2.1. The transverse-axial strain response appears in Figure 2.2.

The axial stress-strain behavior was linear and very repeatable for both the elastic and the failure experiments. The axial tensile modulus E_x of the faceplate was 58.1 GPa (8.43 x 10^6 psi). The transverse-axial strain response was linear in the elastic experiments, but showed signs of non-linearity during

the *1570failure experiment, presumably due to the appearance of damage in the 90° and 45° plies. The average value of the Poisson's ratio of the laminate was ν_{xy} = 0.10. The strength of the faceplates was 9970 MPa (1570 ksi). Failure occurred in the gage section.

2.2. *Transverse Behavior of the Sandwich Material*

In the fracture experiments that follow, the loading is nominally tensile or mode I. As a result, the main load on the sandwich was tensile and the transverse sandwich properties were needed for subsequent analyses. Several tension tests were conducted on a section of sandwich material.

A 25.4 mm (1.0 in) long (unit length) sandwich specimen was carefully cut from the motherboard and machined to the shape and dimensions shown in Figure 2.3a. The specimen was gripped by an adaptor block as shown in the picture: Figure 2.3b. This mechanical attachment was the same that was used later in the fracture experiment. The picture also shows how the half bridge LVDTs, known as DVRTs, were mounted for measurements of the sandwich displacement. These devices are capable of measuring a 0.254 μm (0.00001 in) change in length over a range of 25.4 μm (0.001 in), and require special mounting. The adaptor blocks attached to the faceplates served to transfer the load into the specimen and provide suitable mounts for the DVRTs. The measuring devices were symmetrically mounted to the cylindrical extensions

on either side of the adaptor. The extensions are long and fine threaded screws, with a small free sliding cylinder and two set-screws on each. The DVRTs were mounted to the cylinders by four, spring-tightened knife-edges. This design made the adjustment of very small axial displacements possible by moving the cylinders, thereby zeroing the DVRTs properly.

The tests were conducted in displacement control at a rate of 0.00508 mm/sec (0.0002 in/sec), the load was measured by 20,000-lb load cell.

Although attempts were made to attach the DVRTs directly to the sandwich specimen, no satisfactory solution was found. Since they were mounted to the adaptor block, displacements of the adaptor had to be accounted for by making use of a dummy specimen. Replacing the sandwich specimen with an aluminum dummy specimen made it possible to determine the stiffness of the adaptor blocks from the known displacement of the dummy specimen. A uniform stress distribution was assumed in the aluminum with no friction between the loaded surface and the adaptor. Strain gages were applied to the aluminum block. Subtracting the strain of the aluminum block from the overall measured strain, revealed the displacements in the adaptor. In subsequent experiments, the overall measured displacement was reduced by this correction value to obtain the true displacement in the core and the faceplates.

The load-strain response of the dummy specimen is shown in Fig 2.4a. The response was linear over the approximately 400-lb range, which corresponds to the range experienced in the fracture experiments. The strains, which were measured by strain gages on both sides of the specimen (L and R) were converted to displacements by multiplying by 50.8 mm (2 in), the length of the dummy specimen. The two strain signals were offset for clarity and, since they increased with the same slope, there was no bending. The inverse slope of the load-displacement response revealed the compliance ($5.38\ 10^{-10}$ m/N) ($9.43\ 10^{-7}$ in/lbs) of the dummy specimen. As a check, the stress-strain response of the dummy specimen resulted in a Young's modulus of 71.9 GPa ($10.4\ 10^{6}$ psi).

At the same time, extensometers measured the overall displacement of the dummy specimen and adaptor block. This response is shown in Figure 2.4b. The response of one extensometer was very linear, whereas the other had some nonlinearity. As a result the overall compliance $6.75\ 10^{-10}$ m/N ($1.18\ 10^{6}$ in/lbs) of the adaptor block and dummy gage was obtained from the mean value of the average from each extensometer over five experiments. Even though a relatively thin aluminum dummy specimen was used, it was still 100 times stiffer than the adaptor block whose compliance was $6.21\ 10^{-9}$ m/N ($1.09\ 10^{-5}$ in/lbs), obtained by subtraction of the two responses.

The load displacement response of the sandwich specimen and adaptor block is shown in Figure 2.5. The responses on both sides were quite linear and there was no bending. The compliance of the sandwich specimen was obtained by subtracting the previously determined compliance of the adaptor block from the overall compliance of the sandwich and adaptor block.

The axial tensile stiffness of the sandwich specimen was: k=190 MPa (29 ksi) with a maximum 1.7% difference between left and right side measurements. In further analysis, this value was used as the stiffness per unit length of the sandwiched faceplates and core.

Failure tests were also conducted on the unit length sandwich specimen in order to determine its strength properties. These experiments were conducted under displacement control, which was applied and measured via the hydraulic actuator and the built in LVDT respectively. The load was introduced by the same adaptor blocks as before, but the local displacement was measured by extensometers (Model #632.12B-20 and #634.12E-24), due to the larger expected displacements. The load-displacement response of the sandwich was again revealed by subtracting out the stiffness of the adaptor blocks. The data from two fracture experiments is shown in Figure 2.6, and was very consistent. The experiment started at an initial load, in order to keep the load wire taught. During the experiment, the specimen exhibited slight

bending, particularly at higher load levels. The failure was interlaminar and occurred at 1910 N (430 lbs), or an average stress level of 5.93 MPa (860 psi).

2.3. *Fracture Experiment*

Three series of fracture experiments were conducted using double cantilever beam (DCB) concepts (see Fig 2.7). In the first series, no reinforcement was applied to the faceplates, but it was soon found that the measured displacements and rotations were too large for a linear theory to be used in data reduction. In the second and third series, symmetric reinforcements were applied to both faceplates in order to increase the stiffness and the strength of the peeled members.

In all cases, the length of the sandwich specimen was 266.7 mm (10.5 in), the width of the core was 12.7 mm (0.5 in). An initial crack was introduced along one faceplate/honeycomb interface by carefully sawing away some of the honeycomb. Its nominal 101.6 mm (4 in) length was then increased, by applying a cyclic load to the specimen in order to produce a sharp crack tip.

The load history that was used in the second and third experiments was essentially standard J integral tests. The specimen was first loaded at a constant displacement rate until the crack started to propagate. Unload-reload cycles were then applied (Fig. 2.8) to determine the compliance at each crack length. The grip displacement was applied and measured via the actuator LVDT at

0.254 mm/sec (0.01in/sec). The reactive load was measured using a 500-lb load cell. The data acquisition and experiment control was accomplished in the same way as before. The crack tip region was observed and recorded through a microscope and video system so that initiation events could be examined later.

The compliance was determined from the recorded load-displacement curves, by taking the initial slope of the loading cycles. Using these data points, the energy release rate was calculated and a comparison with the mathematical model of compliance was made.

The second specimen configuration (Fig 2.9) consisted of a 6.35 mm (0.25 in) thick reinforcing steel bar, bonded to each faceplate. The bars had the same 12.7 mm (0.5 in) width as the faceplate, and had a tab at the end. The loading was introduced by rod ends, which connected the tabs to the loading device. The problem with the second configuration was the strength of the adhesive that was used to bond the reinforcement to the faceplate. A number of different adhesives were used. Some worked at room temperature, but none were successful at high temperature.

The third configuration was more mechanical in nature (Fig 2.10). The width of the faceplates was larger than the core so that the faceplates could be gripped along the edges by the channel-shaped reinforcing bars. Forty-two screws placed every 6mm ensured reasonably uniform gripping of the

faceplates. This reinforcement had much larger moment of inertia than the previous one, a much lower compliance, and the temperature distribution was also more uniform.

Since this configuration was used for high temperature experiments and because the robust reinforcement obscured the crack tip, it was not possible to follow the change of crack length through the microscope. Therefore a compliance vs. crack length calibration was made, where the compliance was measured for known crack lengths by carefully sawing the crack in half inch intervals. A typical set of load-displacement responses at 23°C is shown in Figure 2.11a. Five loading/unloading cycles are shown for a short crack and a long one. The responses at each crack length were quite consistent. Because the load-displacement behavior of the specimen was not linear, and the compliance close to critical load was different from the value at low loads, the calibration procedure had to be conducted at elevated load levels. The compliance was obtained from the slope of the loading portion of the cycles as shown in Figure 2.11b, which is the calibration data for 180°C. This calibration was then used to determine crack length from compliance measurements that were made during the fracture experiments.

This rather heavy reinforcement caused some bending in the long adaptor bar that was used to keep the load cell out of the temperature cabinet. The use

of the long bar could not be avoided, since some of the experiments were conducted at high temperature inside the oven. To eliminate this disturbing gravity effect, the free end of the specimen was supported by a fixed length wire that was attached to the top of the adaptor bar, just bellow the load cell. With a turn buckle, the level of the DCB specimen was set to be horizontal before each experiment, without disturbing the measured load data.

2.4. Fracture surfaces

Two fracture mechanisms were observed in the various experiments that were conducted. One will be referred to as adhesive (Fig. 2.12a) because the titanium core pulled out cleanly from the adhesive. The second way that separation occurred was within the faceplates, so that failure was cohesive in the faceplates. This can be seen clearly in Figure 2.12b where the cores are plugged with composite and adhesive and the brown adhesive is missing from the composite faceplate in some locations.

When the second reinforcing configuration was used, failure was almost entirely (70%) cohesive. Furthermore, crack growth was stick-slip in nature, accompanied by sudden changes in load. The third reinforcing configuration gave rise to predominantly adhesive (70%) separation at room temperature. The high temperature resulted in entirely adhesive fracture.

CHAPTER THREE

Mathematical Models

Several analytical models were developed for analyzing the data generated in the experiments described in Chapter 2. First there was an analysis for modeling the stiffness of the core material. Then several beam analyses were used to analyze the different fracture experiments that were conducted. The last of these was a beam on elastic foundation analysis that made use of the core stiffness analysis. Finally the energy release rates in the specimens were related to changes in compliance.

3.1. Analyses of Honeycomb Core

Strength of materials analyses were used to provide bounds for the measured axial elastic behavior of the titanium core. Even though the actual cell structure was neither cylindrical, nor hexagonal, two models were developed based on cylindrical cell structure (see Fig 3.1). First, considering that each element of the core is a single unrestrained cylinder, it can be shown that the stiffness is

$$k_{\max} = \frac{2\pi RtE_c}{h_c}\frac{A_0}{A_1} \qquad (3.1)$$

where R is the radius of the cylinder,

t is the wall thickness of the cylinder,

E_c is the Young's modulus of the cylinder and

h_c is the height of the cylinder (0.89 in).

A_0/A_1 is the number of cylinders in a unit length of a 0.5 in wide specimen.

Going to the other extreme and constraining the cylinder from hoop and radial strains leads to

$$k_{\min} = \frac{2\pi R t E_c}{h_c} \frac{A_0}{A_1} \frac{(1-\nu_c)}{(1-2\nu_c)(1+\nu_c)}, \qquad (3.2)$$

where ν_c is the Poisson's ratio of the core material.

Applying the values in Table 1 to equations (3.1) and (3.2), yields stiffness values of: $k_{\max} = 229.69\,\text{MPa}$ ($0.35008*10^5$ lb/in/in), and $k_{\min} = 155.02\,\text{MPa}$ ($0.23628*10^5$ lb/in/in). These values were applied into the models that follow, and provided reasonable bounds on fracture specimen compliance and therefore good bounds on core stiffness.

Table 1. Elastic Properties and Geometrical Parameters of the Sandwich Material.

Material	Modulus (GPa) (10^6 psi)	Poisson's Ratio	Thickness (t) (mm) (in)	Height (h) (mm) (in)	Radius (R) (mm) (in)
Composite Faceplate	58.083 8.43	0.10	1.27 0.05		
Titanium Core	110.24 16.00	0.33	0.1524 0.006	22.606 0.89	4.445 0.175

3.2. *Analyses of Unreinforced Fracture Experiments*

The first two series of experiments were conducted with no reinforcement of the faceplates. Since the stiffness of the faceplate was much less than that of the core, the delaminating faceplates were considered to be cantilevered along the crack front (Fig. 3.2a). In this case the load is:

$$P = E_f b \Delta \left(\frac{h_f}{a} \right)^3, \tag{3.3}$$

where P is the load,

E_f is the tensile modulus of the faceplate (measured earlier),

b is the specimen width,

Δ is the applied end displacement,

h_f is the faceplate thickness and

a is the crack length.

As can be seen in Figure 3.2b, the beam theory prediction was slightly stiffer than the measured responses, due to the fact that the faceplate was considered to be cantilevered at the crack tip without any opportunity to rotate.

From these experiments, it was clear that larger loads would lead to damage in the faceplates prior to debonding. As a result, some reinforcement of the faceplates would be required in order to examine core to faceplate debonding.

3.3. Reinforced Faceplates

The faceplates were stiffened by bonding them to steel bars. Initially, the steel bar on the bottom plate was 4 times thicker the top one. The bending stiffness of the composite (steel bar plus faceplate) was taken to be that of the steel. This was due to the greater axial modulus and thickness of the steel. The Young's modulus of the steel 206.7 GPa (30×10^6 psi) was almost four times greater than that of the composite faceplate material 58.08 GPa (8.43×10^6 psi). Even for the most slender stiffening case, the moment of inertia of the

stiffening bar was 125 times greater than that of the faceplate due to the different thickness values ($h_s = 0.125 in$, $h_f = 0.05 in$).

Two models were considered. The first one follows equation (3.3) with E_s and h_u substituted for E_f and h_f. This essentially assumes that the bottom steel bar was rigid. The compliance of the bottom bar was taken into consideration in the second model (see Fig. 3.3a), where:

$$P = \frac{E_s b \Delta}{\left[\left(\frac{a}{h_u}\right)^3 + \left(\frac{a}{h_l}\right)^3\right]}, \qquad (3.4)$$

where h_u is the thickness of the upper steel bar and

h_l is the thickness of the lower steel bar.

The measured and predicted load-displacement response is shown in Figure 3.3b. The stiffest response was the one predicted by equation (3.3) with the steel properties and geometry of the upper bar. This is expected because the lower bar was taken to be rigid. The prediction from equation (3.4) was closer to the measured values, but still stiffer. The different stiffness in the measured

stiffness values was due to delaminations between the upper faceplate and its reinforcement. Nonetheless, the gap between predictions and measurements seen here was less than that seen in Figure 3.2b, which suggests that the reinforcements were activating the stiffness of the core. This led to the third model, a beam on an elastic foundation that was to account for the stiffness of the core.

In order to simplify the analysis, the upper and lower reinforcements were made the same. The symmetry leads to a more nearly mode I condition for an interface crack between the core and the faceplate. The elastic property mismatch between the core and the faceplate provides some mode-mix. Larger mode-mix values can be introduced later by returning to asymmetric stiffening.

With reference to Figure 3.4, the governing equation for the analysis is:

$$E_s I_s \frac{dv^{iv}}{dx^{iv}} + kv = q(x), \tag{3.5}$$

where v is the beam displacement,

k is the foundation stiffness per unit length and

$q(x)$ is a distributed lateral loading.

When there is no lateral loading, the solution is:

$$v(x) = e^{\mu x}(C_1 \sin \mu x + C_2 \cos \mu x) + e^{-\mu x}(C_3 \sin \mu x + C_4 \cos \mu x), \quad (3.6)$$

$$\text{where } \mu = (\frac{k}{4EI})^{1/4} \quad (3.7)$$

This equation can be solved by enforcing the necessary boundary conditions, such as the shear and moment being zero at the free ends. The boundary conditions for a beam on an elastic foundation of length L_2 are:

$$M(x_2 = 0) = 0 ,$$

$$V(x_2 = 0) = 0 ,$$

$$M(x_2 = L_2) = -M_0 = -PL_1 ,$$

$$V(x_2 = L_2) = -P , \quad (3.8)$$

and P is the lateral force acting at $x_2=L_2$. The equations for the bending moment and shear force are:

$$\frac{m(x)}{-EI} = v''(x) = 2\mu^2 e^{\mu x}(C_1 \cos \mu x - C_2 \sin \mu x) + 2\mu^2 e^{-\mu x}(C_4 \sin \mu x - C_3 \cos \mu x)$$

$$\frac{V(x)}{-EI} = v'''(x) = 2\mu^3 e^{\mu x}[C_1(\cos\mu x - \sin\mu x) - C_2(\sin\mu x + \cos\mu x)] +$$

$$+2\mu^3 e^{-\mu x}[C_3(\sin\mu x + \cos\mu x) + C_4(\cos\mu x - \sin\mu x)] \qquad (3.9)$$

Applying the boundary conditions (3.8) in equations (3.9) yields a system of four equations for the constants (C_1, C_2, C_3, C_4).

$$[E]\{C\} = \{L\}, \qquad (3.10)$$

where

$$E = \begin{bmatrix} 1 & 0 & -1 & 0 \\ e^{\mu x}\cos\mu x & -e^{\mu x}\sin\mu x & -e^{-\mu x}\cos\mu x & e^{\mu x}\sin\mu x \\ 1 & -1 & 1 & 1 \\ e^{\mu x}(\cos\mu x - \sin\mu x) & -e^{\mu x}(\sin\mu x + \cos\mu x) & e^{-\mu x}(\sin\mu x + \cos\mu x) & e^{-\mu x}(\cos\mu x - \sin\mu x) \end{bmatrix},$$

$$L = \begin{Bmatrix} 0 \\ \dfrac{-M_0}{2\mu^2 EI} \\ 0 \\ \dfrac{-P}{2\mu^3 EI} \end{Bmatrix}, \qquad \text{and} \qquad C = \begin{Bmatrix} C_1 \\ C_2 \\ C_3 \\ C_4 \end{Bmatrix}.$$

The actual specimen consists of a delaminated section and a section where the faceplates are supported by the core (Figure 3.5). The load-displacement

behavior of the actual specimen is obtained by combining the cantilever and the beam on elastic foundation analyses. After calculating the end displacement (at $x_2 = L_2$) and rotation of the beam on the elastic foundation and calculating the end displacement of a simple cantilever beam at $x_1 = L_1$, the overall displacement can be calculated by combining the two models with the kinematic linking conditions:

$$v_1(0) = v_2(L_2) \text{ and } v_1'(0) = v_2'(L_2) \tag{3.11}$$

Assuming that the following trigonometric substitutions can be made due to small rotations, the overall displacement becomes (Fig.3.6):

$$\delta_B = a + a' + b' = a + L_1 \tan\alpha + b\cos\alpha$$

if $\alpha << 1$ then: $\tan\alpha \cong \alpha$, $\cos\alpha \cong 1$,

and $a = v_2(L_2)$, $\alpha = v_2'(L_2)$, $b = v_1(L_1)$,

so that $\delta_B = v_2(L_2) + L_1\alpha + v_1(L_1)$. (3.11)

In this notation L_1 is actually the crack length. Varying it from the initial 3.5 in to the final 6.5 in, and considering, that $L_1 + L_2 = L = 10.5$ in, the compliance was calculated versus crack length. In these calculations, the

measured core stiffness k = 507.5 Mpa (73.661 ksi), was applied, as well as the predicted bounds on k.

3.4. Fracture Aalysis.

Energy release rates were determined on the basis of compliance through:

$$G = \frac{P^2}{2b}\frac{\partial C}{\partial a}, \qquad (3.13)$$

where: P load,

b width of fracture surface (0.5 in),

C Compliance of the system,

a crack length.

The toughness G_c was obtained from the critical load, P_c, at which the crack propagated through:

$$G_{cr} = \frac{P_{cr}^{\ 2}}{2b}\frac{\partial C}{\partial a} \qquad (3.14)$$

The derivative of the compliance was taken as the mean value of the slopes determined from the data points before and after the current point.

$$\left(\frac{\partial C}{\partial a}\right)_i = \frac{1}{2}\left[\left(\frac{\partial C}{\partial a}\right)_{i1} + \left(\frac{\partial C}{\partial a}\right)_{i2}\right], \tag{3.15}$$

where $\left(\frac{\partial C}{\partial a}\right)_{i1} = \frac{C_i - C_{i-1}}{a_i - a_{i-1}}$,

and $\left(\frac{\partial C}{\partial a}\right)_{i2} = \frac{C_{i+1} - C_i}{a_{i+1} - a_i}$.

CHAPTER FOUR

Results and Discussion

The results from the fracture experiments and their associated analyses are now presented. These include load-displacement data, compliance data and fracture toughness data at 23 and $180\,^{\circ}C$. The presentation of results is followed by some discussion and conclusions.

4.1 Load-displacement data.

Typical load-displacement responses at $23\,^{\circ}C$ are shown in Figure 4.1a. The early interruptions to the loading were made in order to check for crack growth prior to any load drop. In these experiments, crack growth was detected on the third reloading. In subsequent experiments, unloading was performed after some crack growth occurred.

During the fracture tests, the unload-load cycles exhibited hysteresis, probably due to the time dependent behavior of the structure. The hysteresis loop increased as the crack length increased. During the first few loops there was no significant difference between the unloading and loading curves, and as one can observe on the load-displacement data, the hysteresis grew to a fairly large amount. It was interesting to observe, that the unloading part of these cycles were much close to linear behavior than the loading parts. The

loading part showed a high degree of non-linearity. The hysteresis behavior was quite similar at 180 °C . At both temperatures, the compliance of these loops was taken to be the initial slope of the loading response.

4.2 Compliance data

The compliance of the calibration specimens with mechanically attached reinforcement is shown in Figure 4.2. The data is for the specimens whose cracks were introduced by saw cuts. This led to a high degree of confidence in the crack length measurements which could be made to within 1.27 mm (0.05 in). The plotted values of compliance were normalized by the compliance of an uncracked specimen at 23 °C (8.0166 10^{-8} m/N) (0.00014045 in/lb), based on the elastic foundation analysis. Crack lengths were normalized by the full crack length of the specimen 266.7 mm (10.5 in). The predicted values of compliance were based on the elastic foundation analysis (equation 3.12) and the stiffness of the sandwich tension specimen k=190.47 MPa (29.031 ksi). It can be seen that the measured and predicted compliance values at 23 °C were in very good agreement. The elastic foundation analysis resulted in slightly higher compliance values for shorter cracks. It is not clear what reason for this is. Adding shear displacements to the cantilever beam would make the difference greater. The bounds were based on analyses of the single and constrained cylinders. The compliance of the specimen at 180 °C was slightly

higher. There was no analysis to compare these results with, because sandwich tension tests could not be conducted at $180\,°C$ with the necessary displacement measurements. None of the available extensometers function at $180\,°C$.

The compliance data for specimens that were used in the fracture experiments is shown in Figure 4.3. There is clearly a greater amount of scatter to this data particularly for larger cracks, so the average of the room and high temperature compliance values are also shown. The amount of scatter is initially surprising considering how consistent the data in Figure 4.2 was. However, the error bars for crack length measurements are much larger, given that it was determined from compliance measurements rather than direct observation. The increase in scatter in compliance values with crack length may also be related to the increased hysteresis and problems with slope determination at larger crack lengths.

Nonetheless, the average compliance of room temperature was slightly lower than the predicted value. As expected, the compliance at $180\,°C$ was the highest. When the slopes of compliance data were used to obtain energy release rates (equation 3.13), the actual compliance of each specimen was used rather than the average values shown in Figure 4.3.

4.3 Toughness data

The toughness of the composite faceplate/titanium core interface is shown in Figure 4.4. The results for $23\,°C$ and $180\,°C$ both appear. The values of toughness in both sets of data decreased with increasing crack length, which is probably due to the end effect, however it is present at shorter cracks as well. The decrease was almost linear and quite dramatic. In Figure 4.5 predicted energy release rates are shown for different overall specimen lengths. These values are based on compliance analyses, and were obtained in the same way as the measured data were processed (equation 3.14 and 3.15) using a unit load. In order to make the results associated with each different overall length comparable, the compliances were normalized by the zero length compliance of each case. The crack length was again normalized by each full length. The fact that the energy release rate values indeed increase much faster with smaller overall length, gives a partial explanation to the drop of toughness data.

The toughness at room temperature was generally higher and was essentially the interlaminar toughness of the faceplates as indicated by the fractograph (Fig. 2.12b) Apparently the bond between the titanium and the faceplate became the weakest link at $180\,°C$ because failure was entirely adhesive (Fig 2.12a).

The data shown in Figure 4.4 all came from specimens whose faceplates were mechanically fastened to the reinforcing beam. There was a much larger degree of scatter when adhesive was used to join the faceplate and reinforcement (Fig 4.6). Any debonding between the faceplate and reinforcement would affect the compliance and introduce an additional source of scatter. The bending stiffness of the bars that were used to provide mechanically attached reinforcement, was also much greater than those that were used for the bonded reinforcement. It is not clear, that this should have any effect.

4.4 Conclusions

The objective of this work was to determine the delamination resistance of the faceplate/core interface in high temperature sandwich panels. The sandwich consisted of composite (IM7/PETI-5) faceplates bonded to titanium honeycomb core with FMx5 film adhesive. The in-plane modulus, Poisson's ratio and strength of the $[45/0/-45/90]_{2S}$ faceplate were determined in a standard tensile test of material that was removed from a panel. The transverse tensile behavior of the faceplate and core was then determined using a specially designed mounting and gripping arrangement. The stiffness of the faceplate/core was later used in beam on elastic foundation analyses of the

fracture experiment. The strength was also determined and may be useful in future analyses.

The main experiment of the work was nominally mode I fracture of the faceplate/core interface. In quickly became clear that the toughness of the bond between the two was such that the faceplate required some reinforcement. It turned out, after trying many different adhesives, that the reinforcement needed to be mechanically joined to the faceplates, particularly at high temperature. Since toughness was determined on the basis of compliance measurements, complementary analyses were conducted to predict compliance. A beam on elastic foundation analysis provided satisfactory agreement with experiment.

Many fracture experiments were conducted at 23 and $180\,^{\circ}C$. The toughness was slightly higher at $23\,^{\circ}C$ and delamination occurred mainly via interlaminar fracture in the composite faceplate. This might have been avoided by using a 0^{0} ply as the outside ply of the faceplate. At $180\,^{\circ}C$ fracture was mainly adhesive with a clean pullout between the faceplate and core. A surprising feature of the toughness values was a noticeable decrease with increasing crack length. This may be due to an end effect for long cracks ($a/L > 0.7$) but was apparent even for quite short cracks.

In making recommendations for future work, it is clear that the high temperature tension test of a sandwich element need to be accompanied by displacement measurements. The stiffness obtained from such an experiment could then be used to make predictions of the fracture specimen compliance at high temperature. The stiffness and strength data from these tension tests could presumably be used in cohesive zone models of delamination process. Such models would than form the basis for durability predictions. Such models could also account for mode-mix effects and, perhaps, explain the apparent drop in fracture with crack length.

Appendix

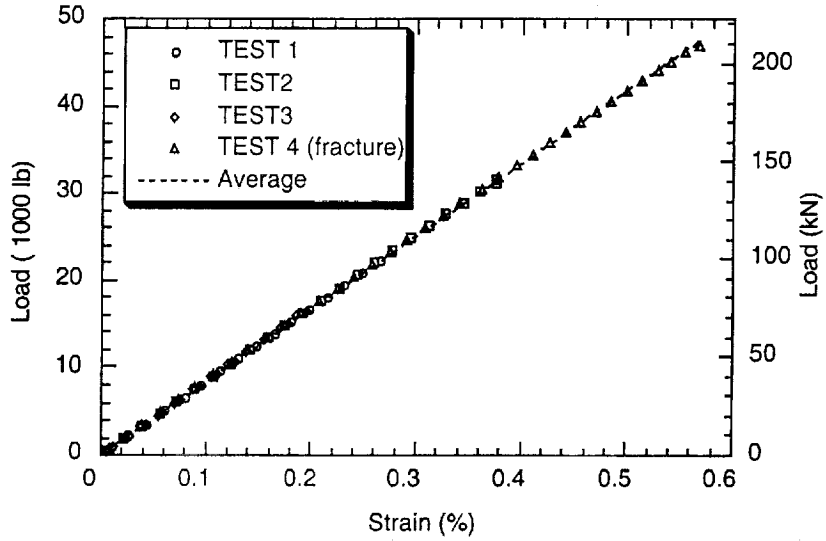

Figure 2.1 Axial stress-strain behavior of the faceplate material $[45/0/-45/90]_{2s}$

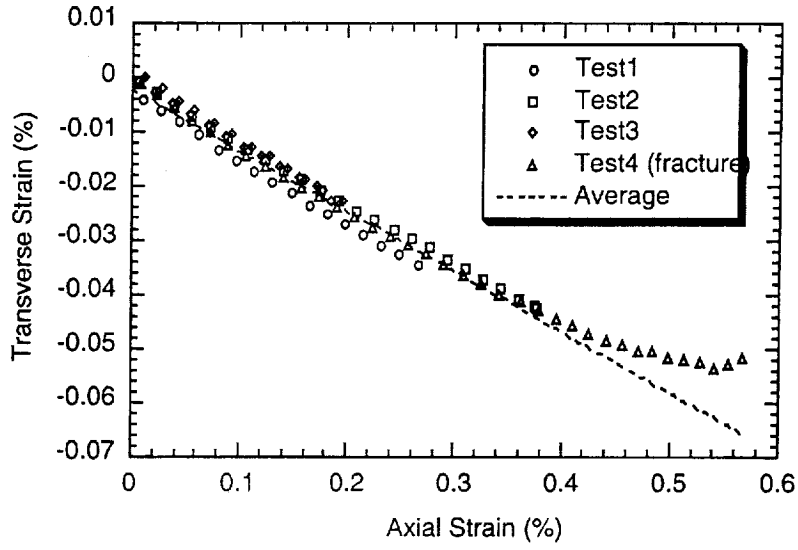

Figure 2.2
Transverse-axial strain behavior of the faceplate material $[45/0/-45/90]_{2s}$

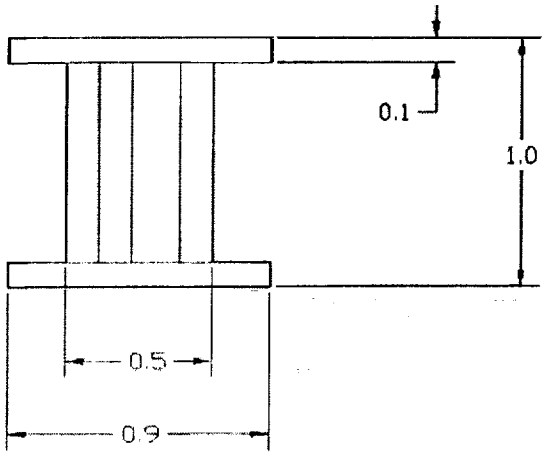

(a)

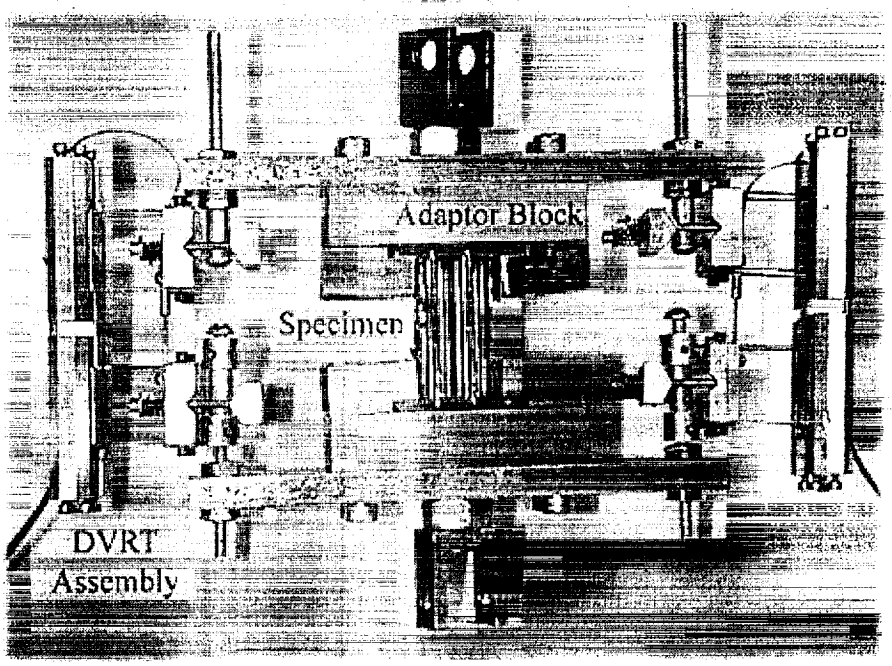

(b)

Figure 2.3 (a) Cross section of sandwich tension specimen; (b) Specimen with adaptor block

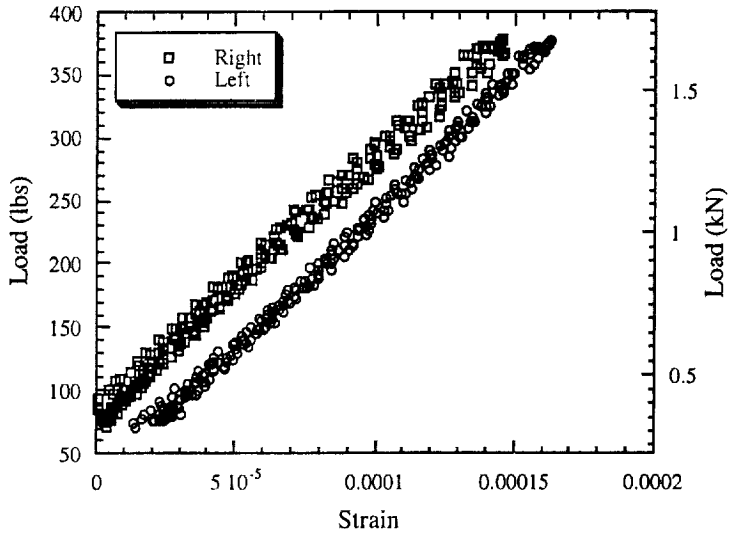

(a)

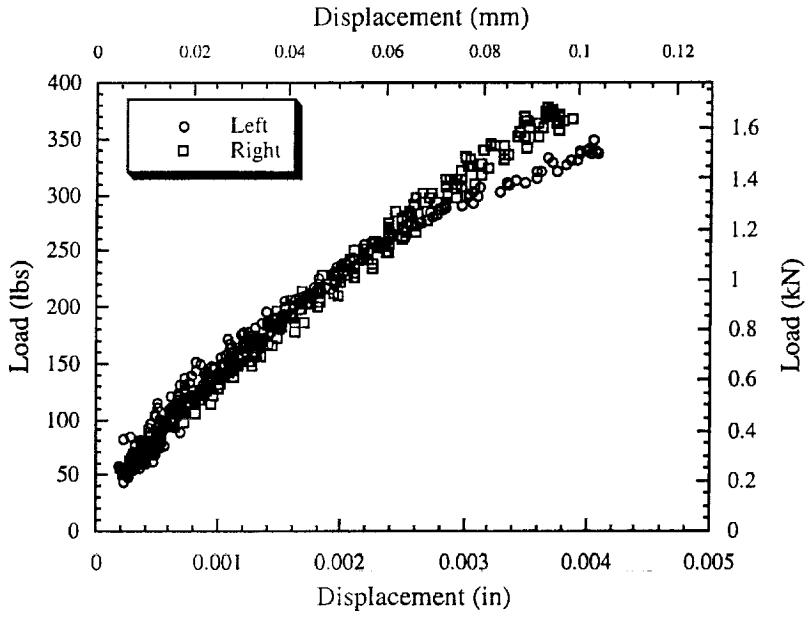

(b)

Figure 2.4 (a) Load-strain response of dummy specimen from strain gages; (b) Overall load-displacement response of dummy specimen and adaptor block.

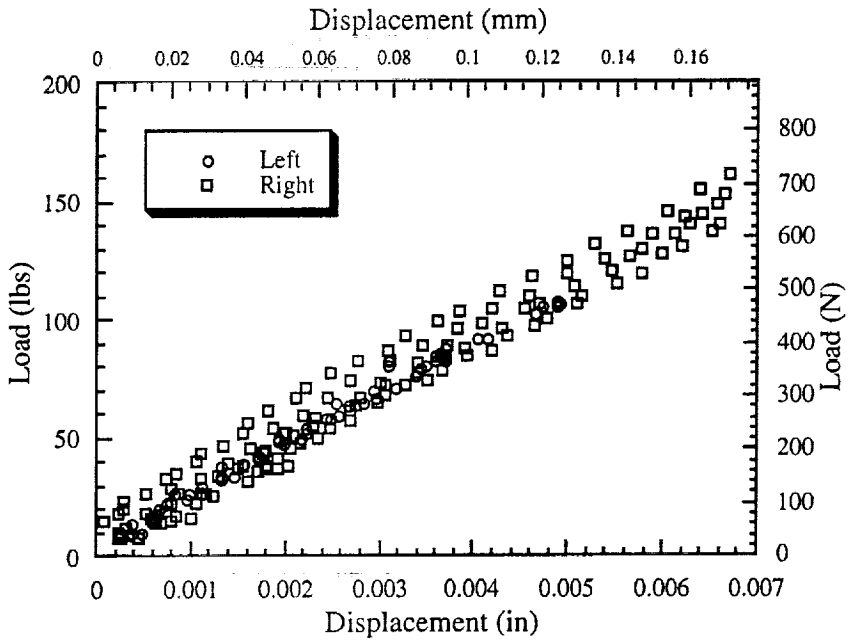

Figure 2.5 Overall load-displacement behavior of sandwich specimen and adaptor block.

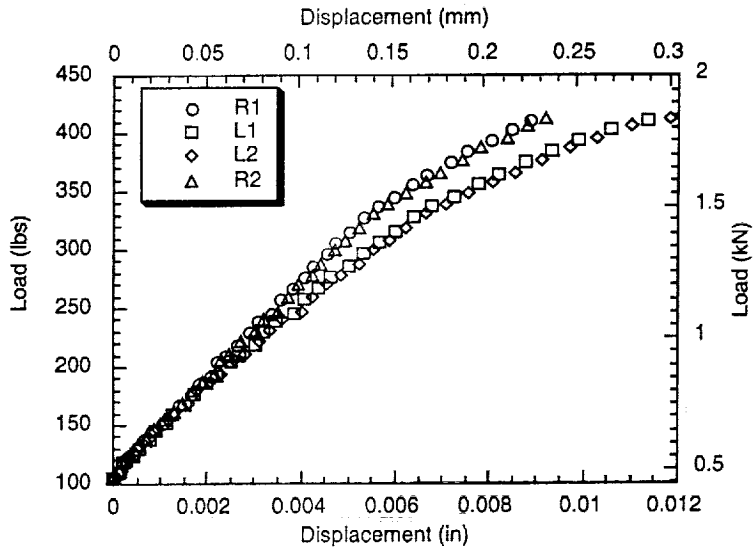

Figure 2.6 Sandwich specimen failure experiment.

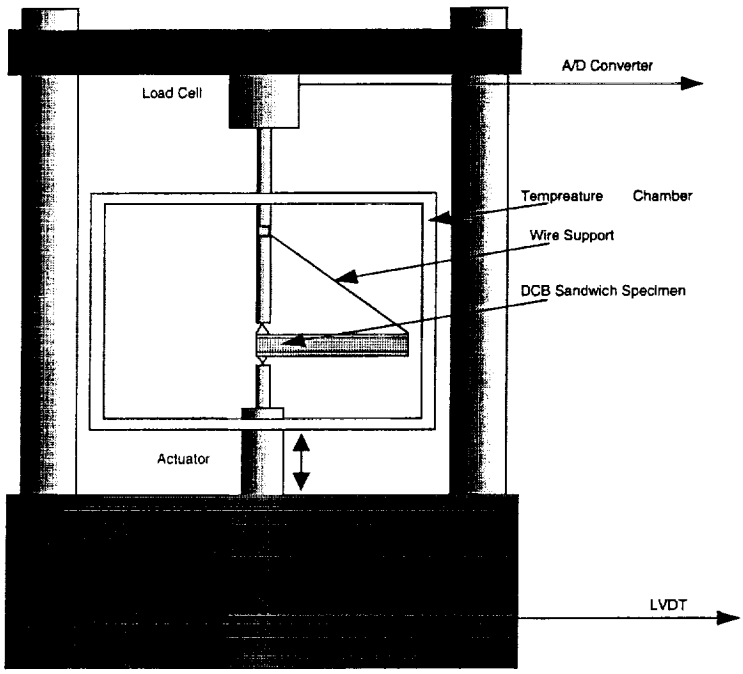

(a)

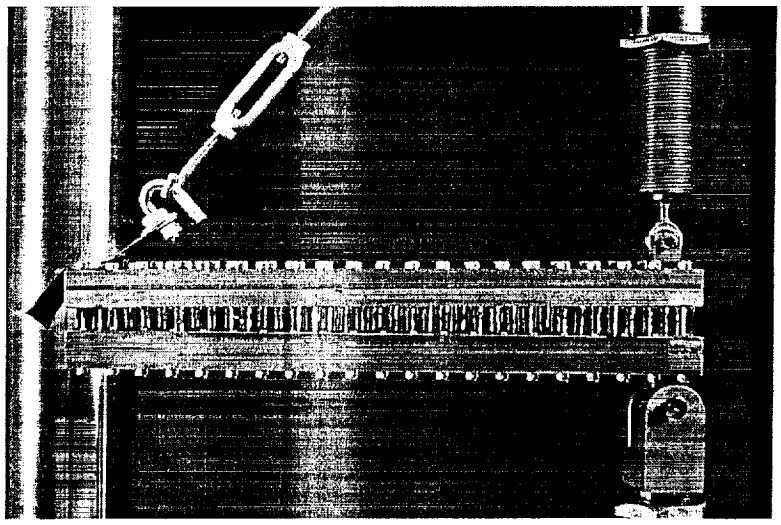

(b)

Figure 2.7 (a) Schematic of fracture experiment; (b) Specimen and gripping.

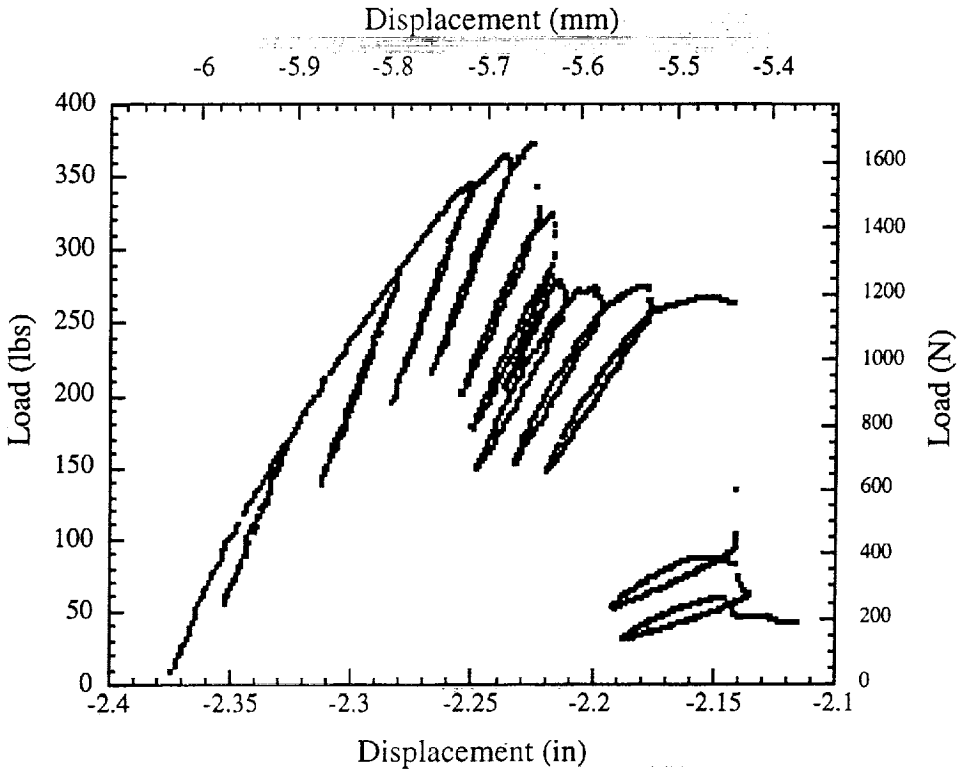

Figure 2.8 Typical fracture test (23 °C, specimen26)

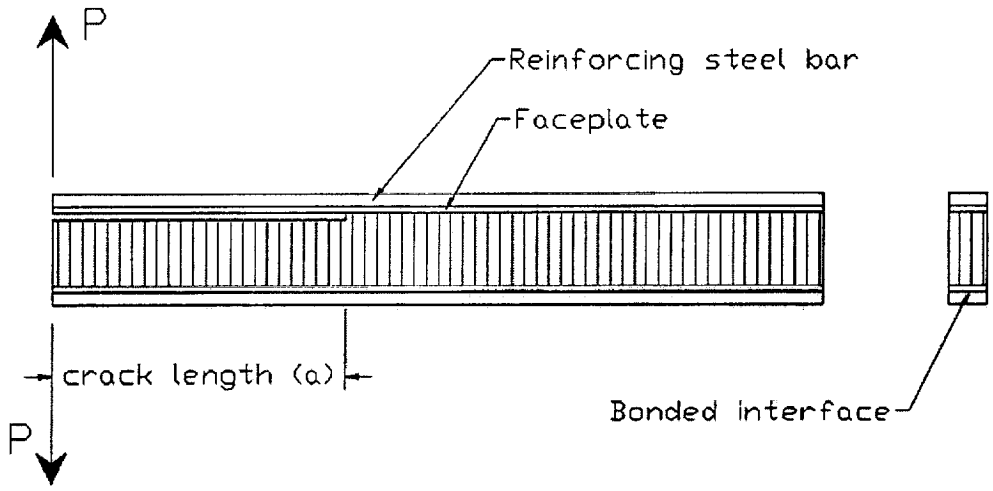

Figure 2.9 Second fracture specimen configuration with bonded reinforcement

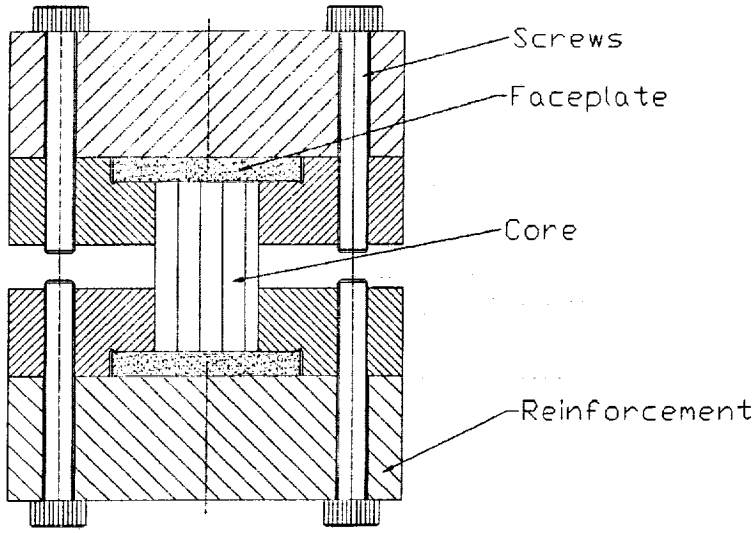

(a)

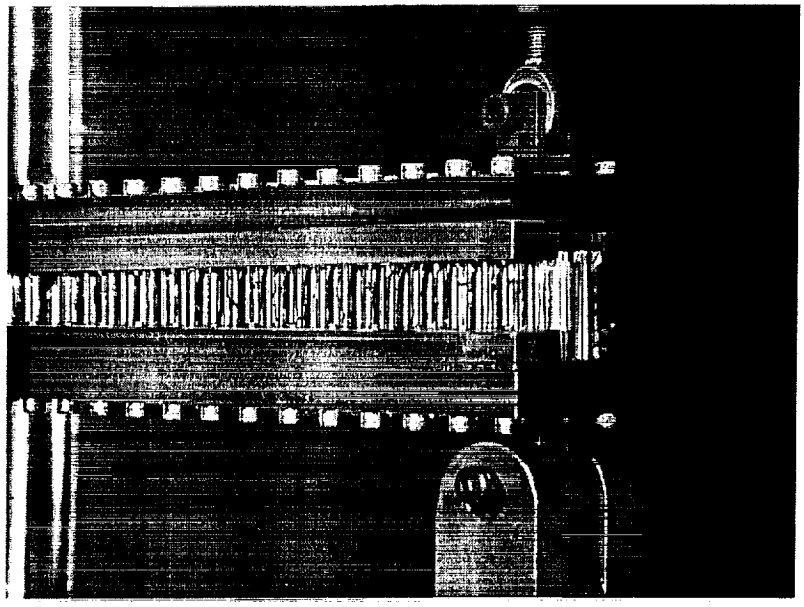

(b)

Figure 2.10 (a) Schematic of fracture specimen gripping; (b)Fracture experiment configuration.

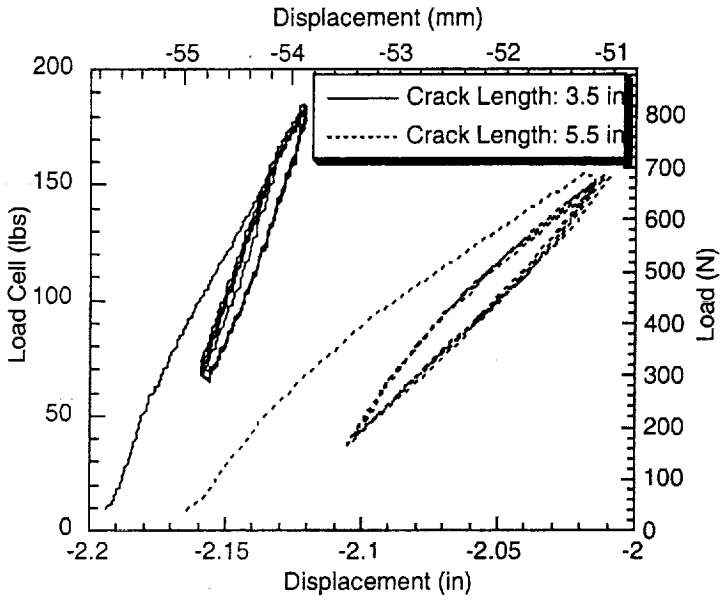

(a)

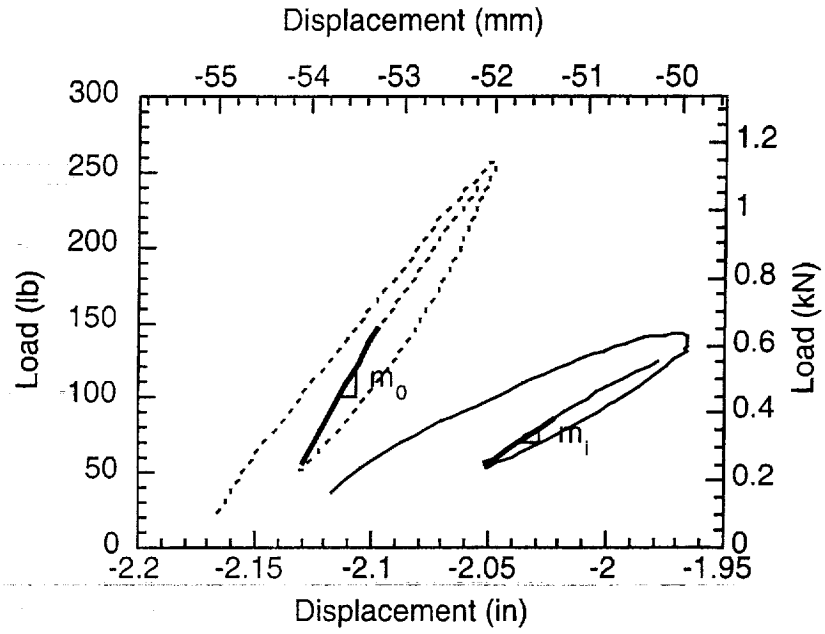

(b)

Figure 2.11 Load displacement response of calibration experiment at (a) 23°C and at (b) 180°C.

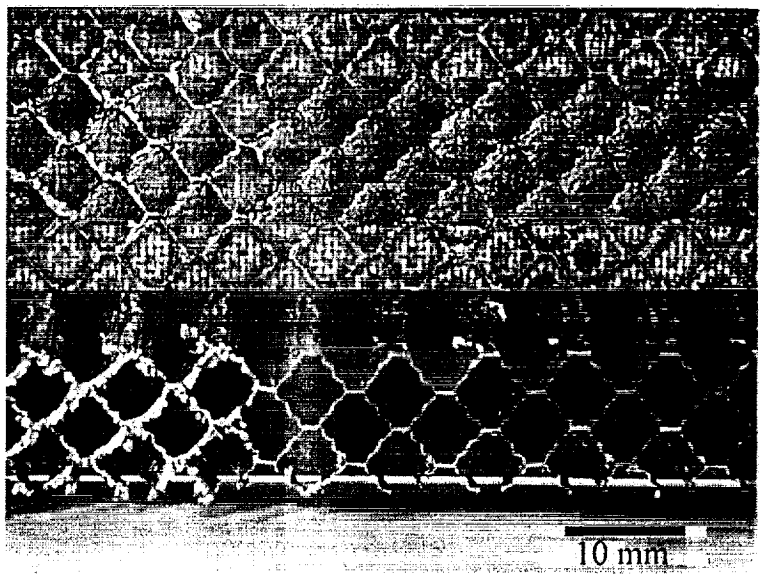

(a)

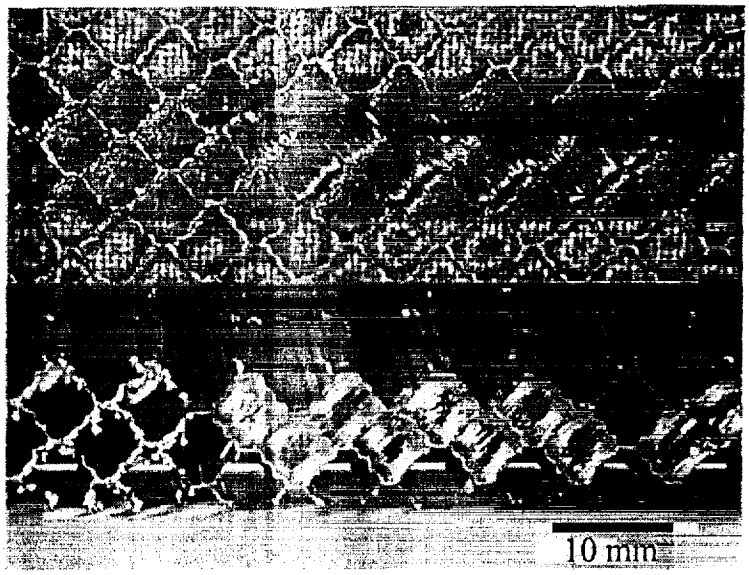

(b)

Figure 2.12 (a) Adhesive and (b) cohesive fracture surfaces.

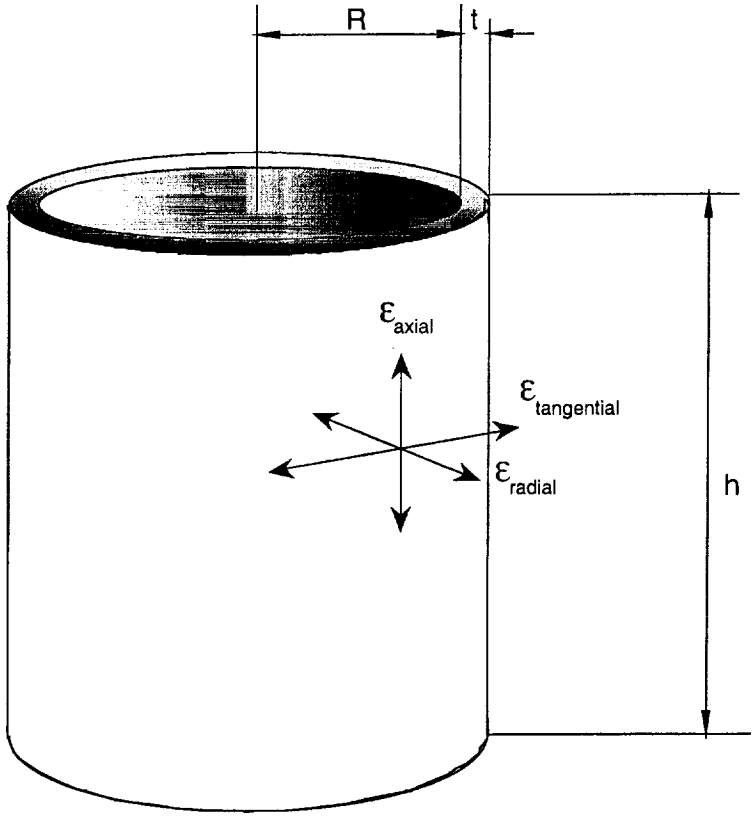

Figure 3.1 Cylindrical Core Model.

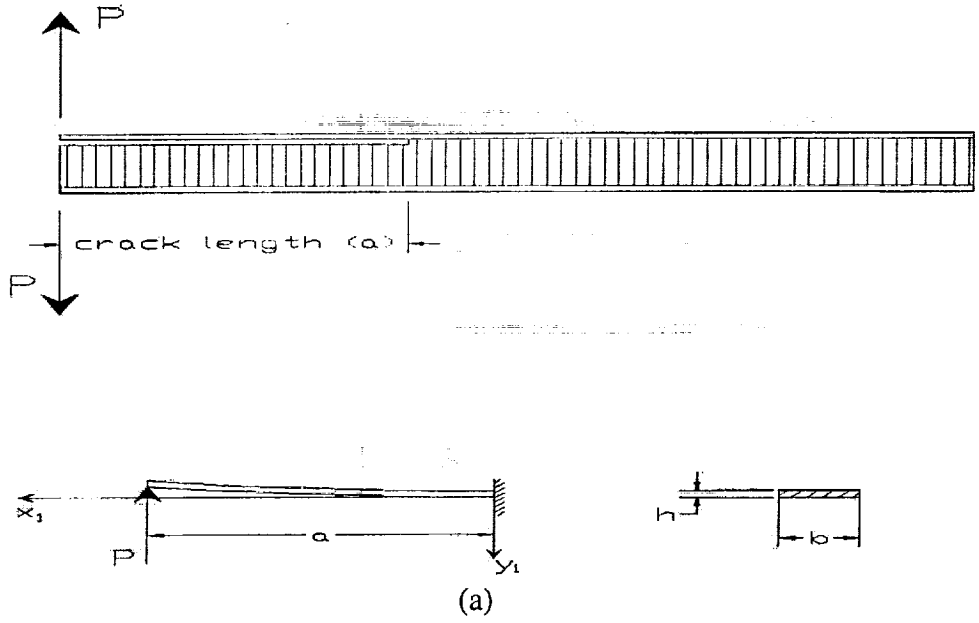

(a)

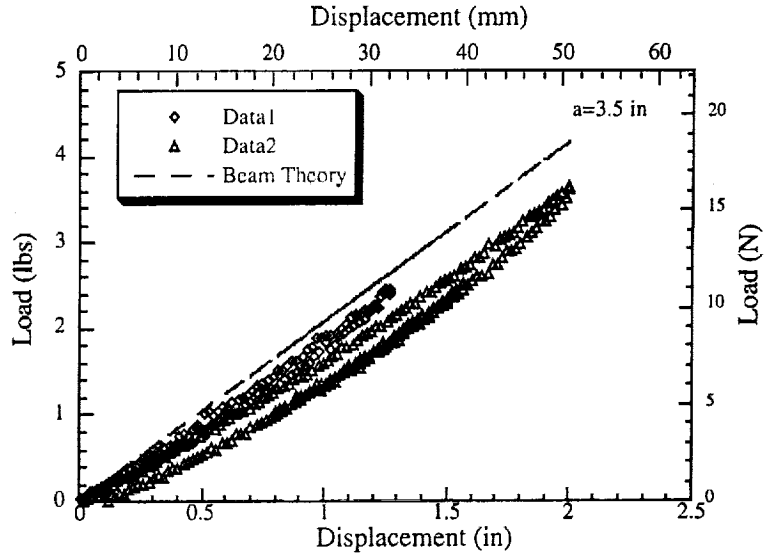

(b)

Figure 3.2. (a) Unreinforced fracture specimen and model; (b) Load-displacement behavior of an unreinforced specimen

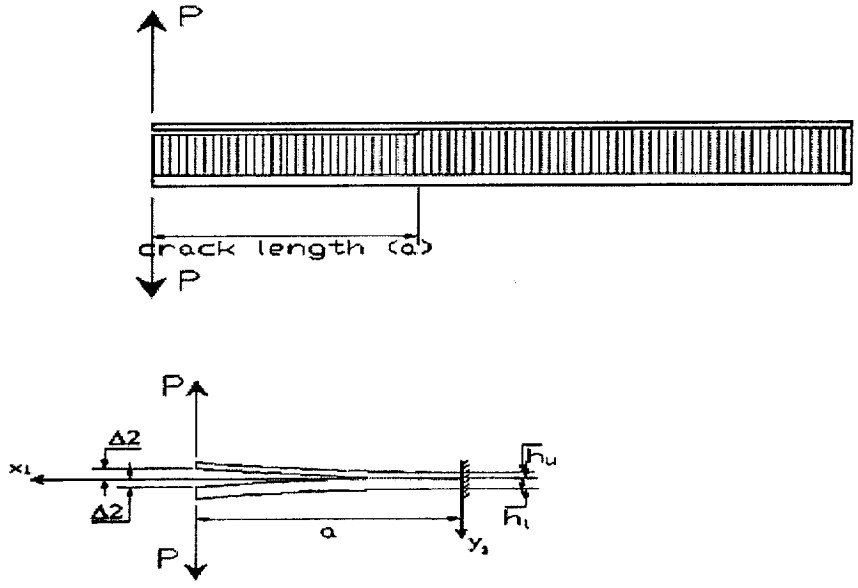

(a)

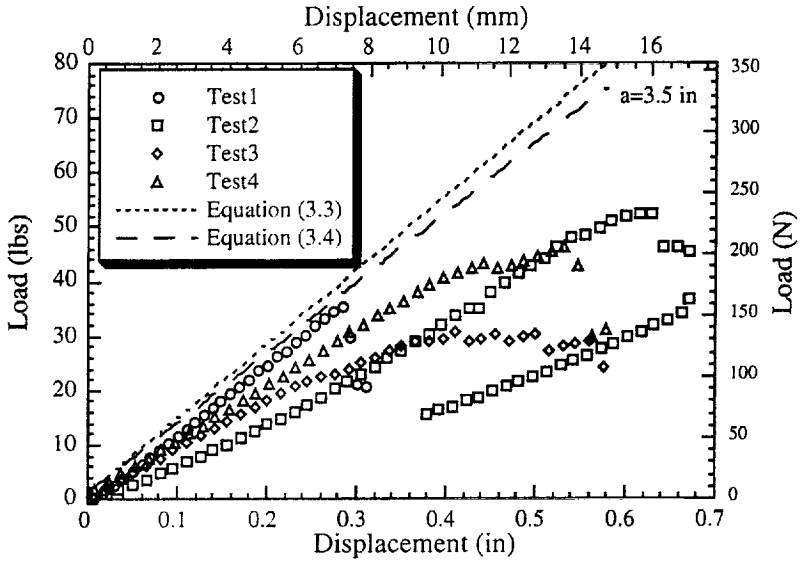

(b)

Fig 3.3 (a) Unsymmetrically reinforced fracture specimen and model; (b) Load-Displacement of an unsymmetric reinforced specimen(a=3.7 in; h_u=0.125 in; h_l=0.25 in; b=0.5 in)

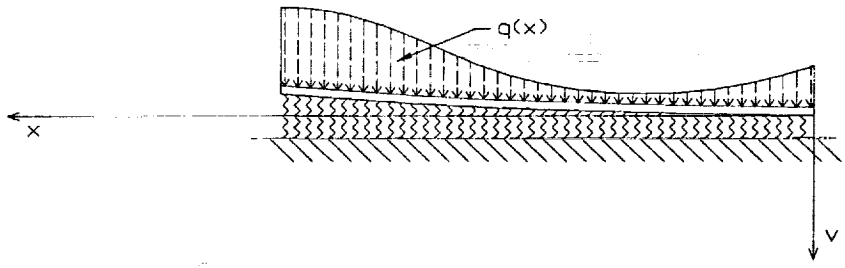

Figure 3.4 Beam on elastic foundation.

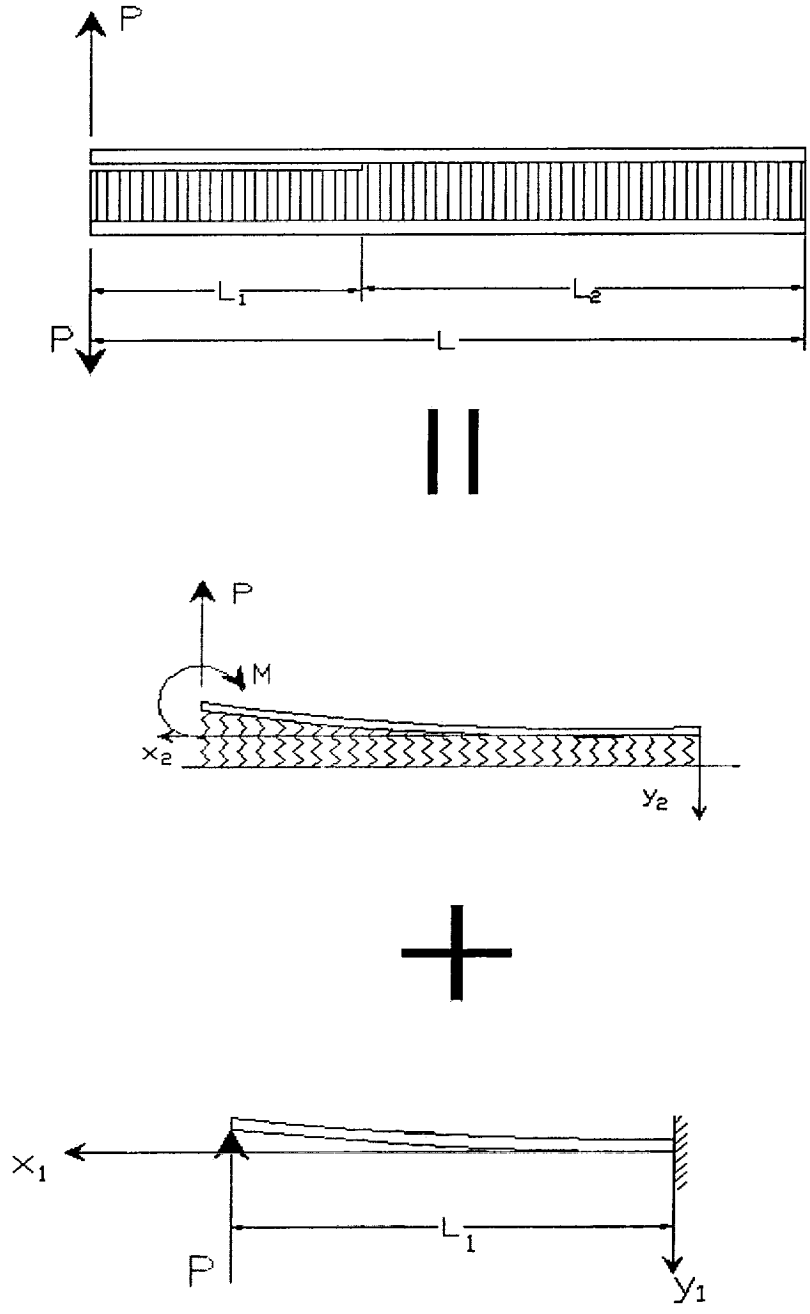

Fig 3.5 Model of symmetrically reinforced fracture specimen.

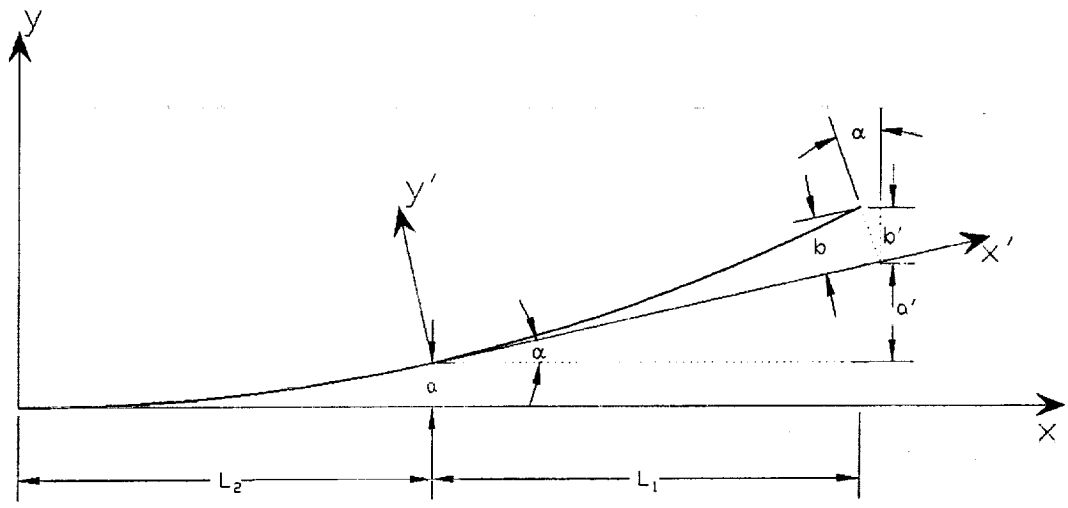

Figure 3.6 Model of tip displacement.

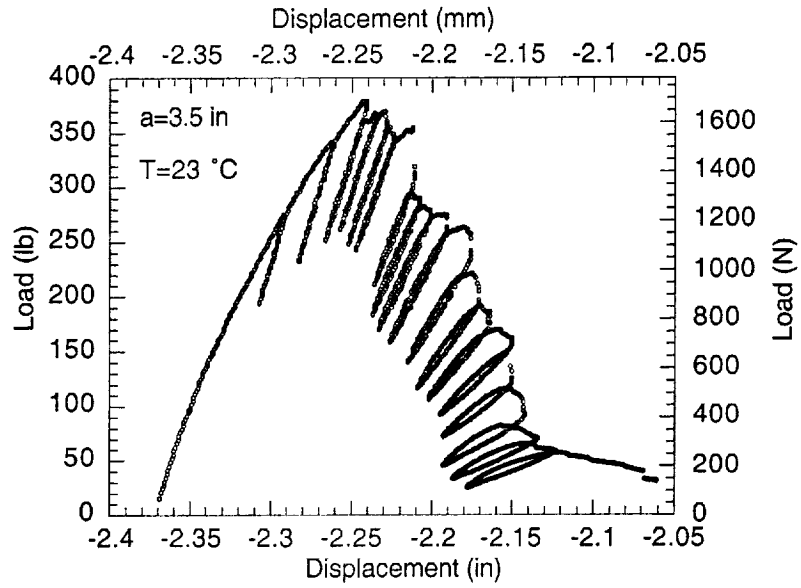

(a)

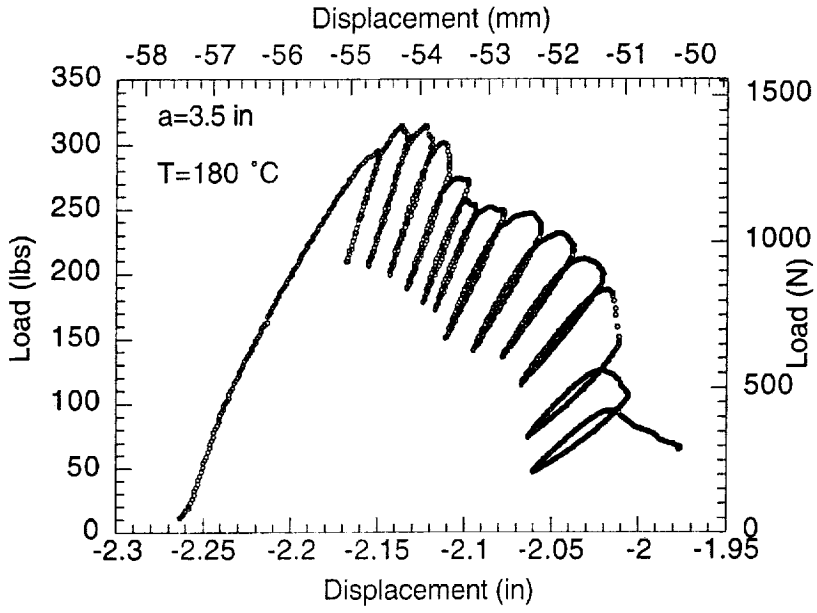

(b)

Figure 4.1 Load-displacement behavior of fracture specimens at (a) 23 °C and at (b) 180 °C.

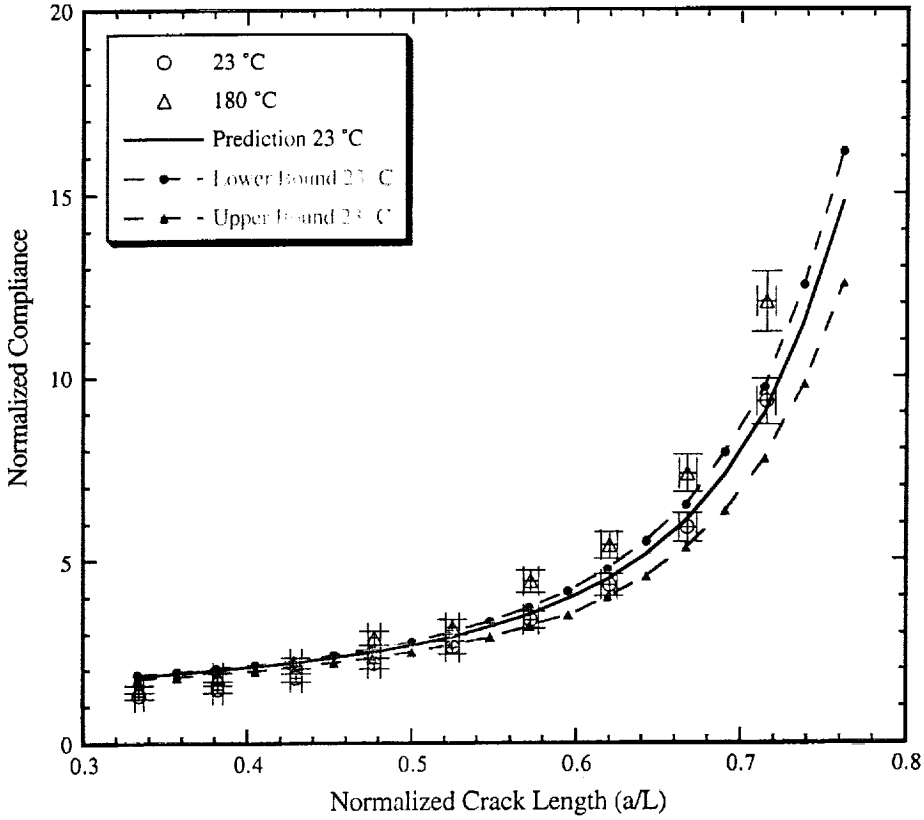

Figure 4.2 Measured and predicted compliance of calibration specimen.

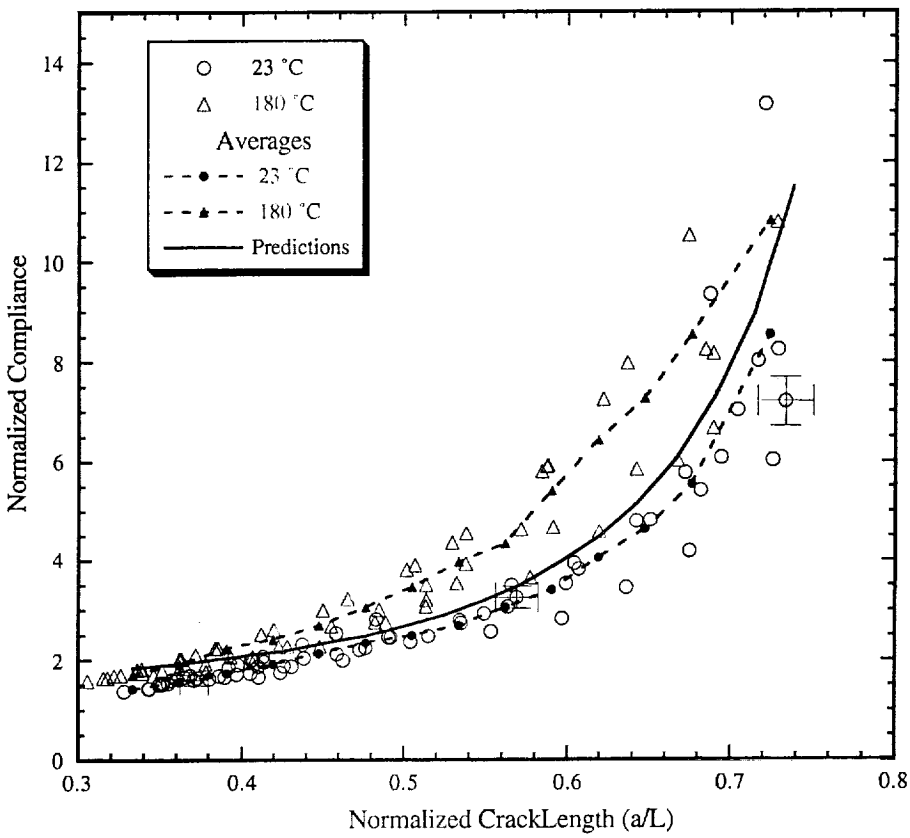

Figure 4.3 Average of room temperature and high temperature compliance data.

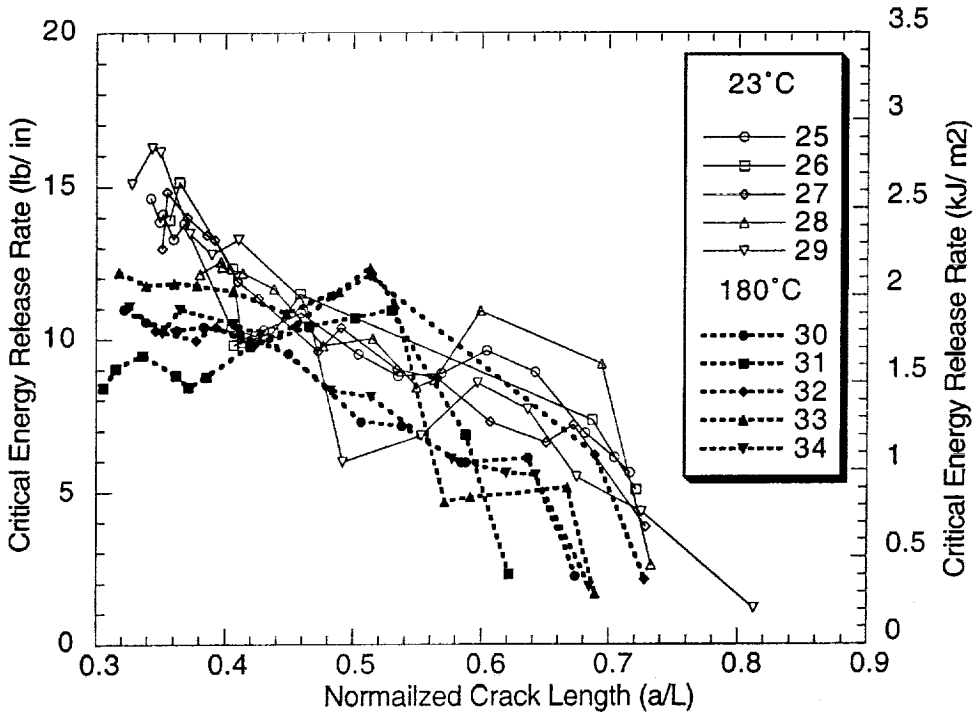

Figure 4.4: Critical energy release rates of robust configuration specimens

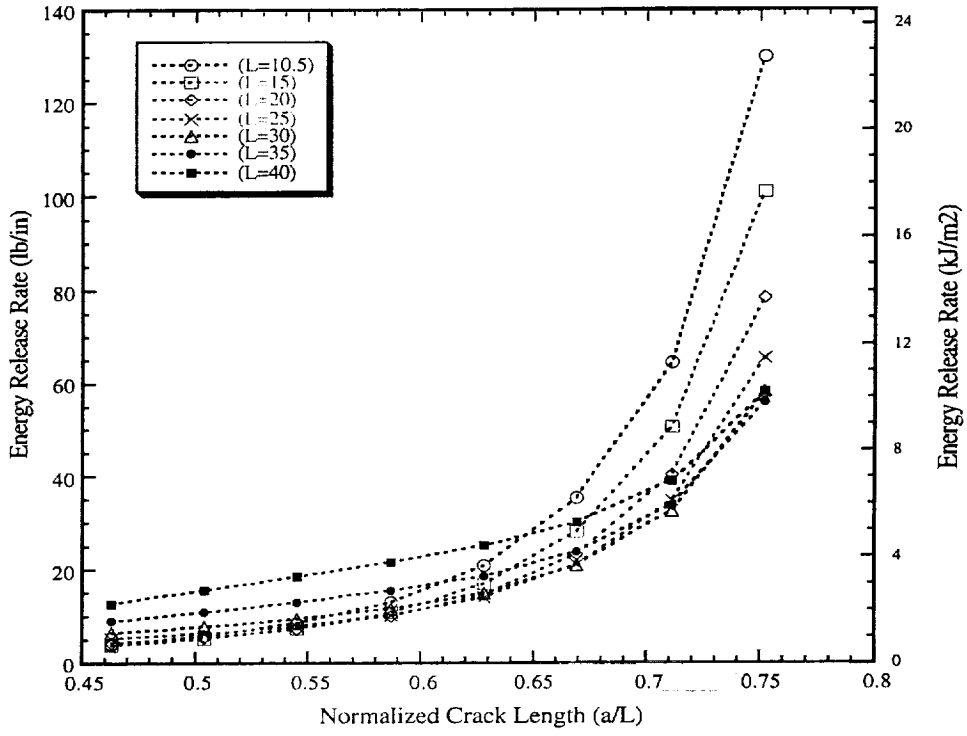

Figure 4.5 Energy Release Rate Prediction

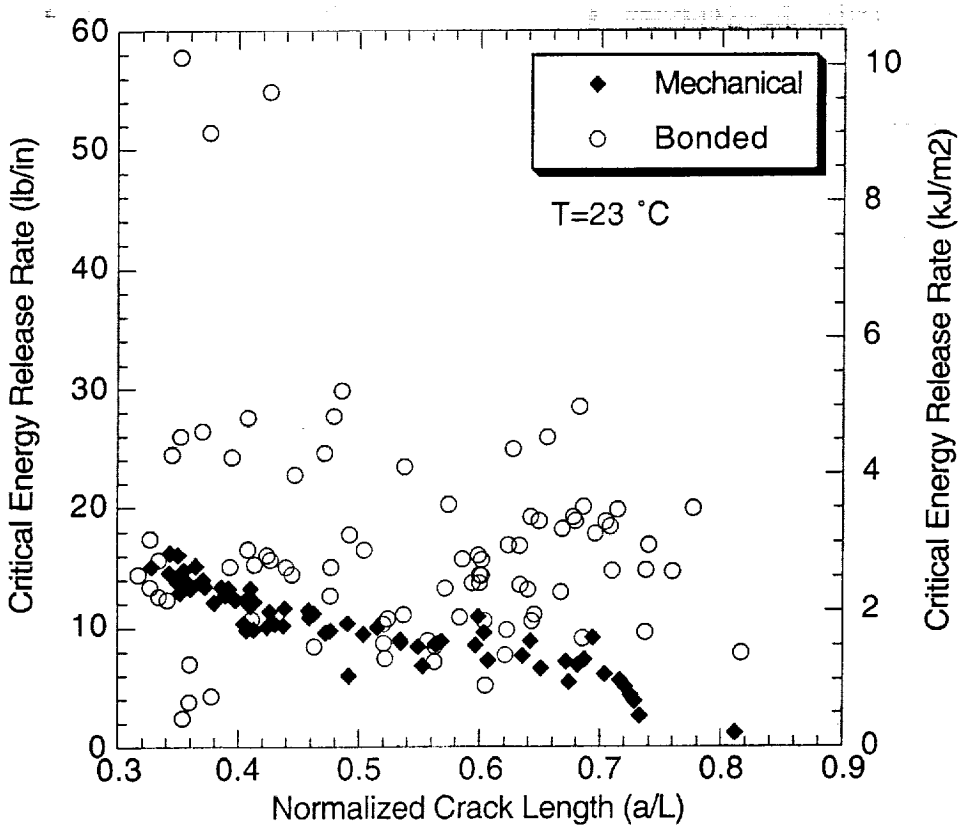

Figure 4.6 Critical energy release rates of all room temperature specimens.

Bibliography

Ahmer, W.M.,1999, "Experimental Evaluation of Interactive Buckle Localization in Compression Sandwich Panels",*Journal of Sandwich Structures and Materials,* Vol.1, pp230-254.

Altenbach, H. ,2000, "An alternative determination of transverse shear stiffness for sandwich and laminated plates",*International Journal if Solids and Structures,* Vol. 37, pp.3503-3520.

Balendran, B.,1994,"On The Double Cantilever Beam Specimen For Mode-I Interface Delamination", *Journal Of Applied Mechanics*, Vol. 61, pp. 471-473.

Bart-Smith, H.; Bastawros, D. R.; Evans, A.G., 1997, "Compressive deformation and yielding mechanisms in cellular Al alloys determined using X-ray tomography and surface strain mapping",

Carlsson, L.A.,1991, "Characterization Of Face Sheet/Core Shear Fracture Of Composite Sandwich Beams", *Journal of Composite Materials*, Vol. 25, pp. 101-116.

Chai, H.,C.D.Babcock and W.G. Knauss. 1981."One dimensional Modelling of Failure in Laminated Plates by Delamination Buckling",*Int.J. Solids Structures*, Vol. 17(11), pp 1069-1083.

Chen, J.Y. and Huang, Y. and Oritz, M.,1998, "Fracture analysis of Cellular materials: A strain gradient model",*Journal of Mech. Phys. Solids,* Vol. 5, pp. 789-828.

Falk, L.,1994, "Foam core sandwich panels with interface disbonds",*Composite Structures*, Vol. 28, pp. 481-490.

Hansen, U., 1998,"Compression Behavior of FRP Sandwich Specimens with interface debonds",*Journal of Composite Materials,* Vol.32, pp335-360.

Kardomateas, G. A.,1988,"Effect Of An Elastic Foundation On The Buckling And Postbuckling Of Delaminated Composites Under Compressive Loads", *Journal Of Applied Mechanics*, Vol. 55, pp. 238-241.

Kassapoglou,C.,P.J.Jonas and R.Abbot.1988."Compressive Strength of Composite Sandwich Plates", *Composite Structures*, Vol. 9, pp. 160-172.

Krajcinovic, D.,1972,"Sandwich Beam Analysis", *Journal of Applied Mechanics*, Vol.39, pp. 773-778.

Li, X. and Carlsson, L. A. (1999) "The Tilted Sandwich Debond (TSD) Specimen for Face/Core Interface Fracture Characterization," *Journal of Sandwich Structures and Materials*, Vol. 1,pp. 60-75.

Llanos, Antonio S.; Vizzini, Anthony J,1992,"Effect Of Film Adhesive On The Delamination Strength Of Tapered Composites", *Journal Of Composite Materials*, Vol. 26 pp. 1968-1983.

Madenci, E.; Westmann, R.A.,1991,"Local Delamination Buckling In Layered Systems", *Journal Of Applied Mechanics*, Vol. 58, pp. 157-166.

Mannion, L. F.,1987,"Energy Release Rate In An Idealized Nonlinear Dcb Specimen", *Journal Of Applied Mechanics*, Vol. 54, pp. 227-228.

Niu, K. and Talreja, R., 1999, "Buckling of a thin layer on Winkler Foundation with Debonds",*Journal of Sandwich Structures and Materials*, Vol. 1, pp. 259-278.

Papanicolaou, G.C.,1995,"Effect of Treatment Conditions on the Mode I Delamination Fracture Toughness Of Sandwich Structures", *Journal of Composite Materials*, Vol. 29, pp. 2295-2316.

Prasad, S. and Carlsson, L.A. (1994) "Debonding and crack kinking in foam core sandwich beams-I. Experimental investigation" *Engineering Fracture Mechanics*, Vol. 47,pp. 825-841.

Prasad, S. and Carlsson, L.A. (1994) "Debonding and crack kinking in foam core sandwich beams-II. Experimental investigation" *Engineering Fracture Mechanics*, Vol. 47,pp. 825-841

Sankar, Bhavani V.; Dharmapuri, Sreerama M.,1998,"Analysis Of A Stitched Double Cantilever Beam", *Journal Of Composite Materials*, Vol. 32, pp. 2203-2225.

Vintilescu, I.; Spelt, J.,1998,"Mixed Mode I, Ii, And Iii Fracture Characterization Of Adhesive Joints", *Journal Of Composites Technology & Research*, Vol. 20 pp. 129-139.

Wool, Richard P.,1978,"Peel Mechanics Of Adhesive Strips With Constraints", *International Journal Of Fracture*, Vol. 14, pp. 597-603.